ELSEVIER

Polymer 42 (2001) 10101–10110

polymer

www.elsevier.com/locate/polymer

Phase behavior, morphology and interfacial structure in thermoset/thermoplastic elastomer blends of poly(propylene glycol)-type epoxy resin and polystyrene–*b*-polybutadiene

Qipeng Guo, Pedro Figueiredo, Ralf Thomann, Wolfram Gronski*

Institut für Makromolekulare Chemie, University of Freiburg, Stefan-Meier-Strasse 31, D-79104 Freiburg, Germany

Received 29 April 2001; accepted 6 August 2001

Abstract

Thermoset/thermoplastic elastomer (TPE) blends of poly(propylene glycol) (PPG)-type epoxy resin (ER) and a diblock copolymer, polystyrene–*b*-polybutadiene (SB, with 30% styrene content), were prepared using 4,4′-diaminodiphenylmethane (DDM) as curing agent. The miscibility and thermal transition behavior of DDM-cured ER/SB blends were investigated by differential scanning calorimetry (DSC) and dynamic mechanical analysis (DMA). The existence of three separate glass transitions, which are independent of the blend composition, indicates that SB is immiscible with DDM-cured ER. Neither the PS block nor the PB block exhibits miscibility with the cured ER. There exist three phases in the blends: a PS microphase, an ER-rich phase and a PB microphase. The phase structure and morphology of the ER/SB blends were studied using both scanning and transmission electron microscopy (SEM and TEM); a variety of morphologies were observed, depending on the blend composition. For the blends with 5 and 10 wt% SB, SB domains with irregular shapes and broadly distributed sizes are dispersed in a continuous cured ER matrix. For the blends with 20–60 wt% SB, interpenetrating bicontinuous phase structures are observed. For the blends with 70 wt% and more SB, a dispersion of cured ER particles in the SB matrix is obtained. The TEM observation showed that the two phases in the blends exhibit a good interfacial adhesion. The interfacial layer between the ER and SB phases varies from 100 to 300 nm for the blend with 20 wt% SB content, SB micelles are formed surrounding the SB domains in the ER matrix. Small-angle X-ray scattering (SAXS) experiments reveal that the SB diblock polymer still exhibits a lamellar microphase structure within the SB phase and the long spacing of lamellae nearly does not change in the blends. The SB diblock copolymer is microphase separated in the macroscopically phase separated ER/SB blends.

Keywords: Epoxy resin; Polystyrene–*b*-polybutadiene; Thermoset/thermoplastic elastomer blends

1. Introduction

Thermosetting polymers are among the most important materials in many industries and being used increasingly in engineering applications. They are generally amorphous, highly-crosslinked polymers, possessing various excellent properties such as high tensile strength and modulus, easy processing, good thermal and chemical resistance and dimensional stability. However, they have low toughness and poor crack resistance, and are hence normally brittle at room temperature. This is the basic reason why a large body of literature has been on the subject of toughening of thermosets by rubbers and thermoplastic polymers [1–4].

However, relatively few systematic studies have been paid to the miscibility, phase behavior and morphology in blends of thermosetting resins with linear polymers [5–18]. The resulting morphology and extent of phase separation is known to affect the final optical and mechanical properties of the cured blends. Therefore, the need for an understanding of the miscibility, phase behavior and morphology in thermosetting polymer blends is of great practical importance [5,6]. Furthermore, it is also of much academic interest to examine these basic aspects of a thermosetting polymer blend system. The interrelationship between the miscibility, phase behavior, morphology and composition in thermosetting polymer blends is complicated and can be remarkably affected by crosslinking [5,6].

Epoxy resins are a major class of thermosetting polymers. Thermoset blends of epoxy resins and linear polymers are extensively studied with an effort to improve fracture toughness of cured epoxy resins as well as to correlate phase behavior, morphology and mechanical properties of the cured blends [19–31]. The linear polymers used can be classified into two main categories: reactive liquid rubbers

* Corresponding author. Tel.: +49-761-203-6276; fax: +49-761-203-6319.

E-mail address: gronski@uni-freiburg.de (W. Gronski).

0032-3861/01/$ - see front matter
PII: S0032-3861(01)00562-6

and high-performance thermoplastics (either reactive or nonreactive). Very little has been published on using thermoplastic elastomers to toughen epoxy resins and hence on the related blends.

In this contribution, we report the results of an investigation on thermoset/thermoplastic elastomer (TPE) blends of poly(propylene glycol) (PPG)-type epoxy resin (ER) and a diblock copolymer, polystyrene–*b*-polybutadiene (SB). SB is a diblock copolymer with 30 wt% styrene content. Thermoset/TPE blends of PPG-type ER, i.e. poly(propylene glycol) diglycidylether (PPGDGE), and SB were prepared using 4,4′-diaminodiphenylmethane (DDM) as curing agent. In particular, the phase behavior, morphology and interfacial structure of the cured blends will be addressed in detail. The chemical structures of PPGDGE and DDM are as follows:

PPGDGE ($n = 4.31$) :

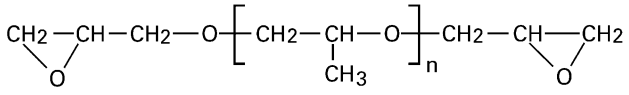

4,4′-Diaminodiphenylmethane (DDM):

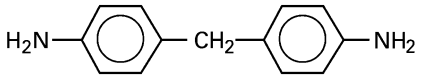

This system is chosen for several reasons. First, the SB diblock copolymer with 30 wt% styrene content is topologically simple compared to SBS triblock copolymers, a widely used TPE. Second, PPG-type ER is less polar than the conventional bisphenol-A-type ER, and hence is expected to exhibit better compatibility with SB. Thirdly, it is interesting to notice that the DDM-cured PPG-type ER has a glass transition temperature (T_g) (33°C by DSC) just in the neighborhood of room temperature, above which it also exhibits characteristics of an elastomer like SB. Finally, the SB does not bear any groups, such as terminated or pendant groups, which may become involved in the curing reaction with DDM. Therefore, the phase behavior in the cured blends cannot be affected chemically or physically by the resultant interchain crosslinking and compatabilization effect of in situ formed copolymers.

2. Experimental

2.1. Materials and preparation of samples

SB diblock copolymer with 30 wt% styrene content had a density of 0.940 g/cm^3 and a weight-average molecular weight $M_w = 68,000$ with $M_w/M_n = 1.12$ as measured by GPC. The uncured epoxy resin used in this study was PPGDGE and had a number-average molecular weight $M_n = 380$. The curing agent used was DDM. All of these materials were purchased from Aldrich Chemicals, Inc., USA.

To prepare the DDM-cured ER/SB blends, the preweighed SB diblock copolymer, PPGDGE and DDM were dissolved in tetrahydrofuran (THF). DDM was used in stoichiometric epoxide/amine ratios relative to the PPGDGE content in the mixtures. The solution was then poured into an aluminum pan and the solvent was evaporated at room temperature. The residual solvent was further removed under vacuum at room temperature. The samples of ternary mixture were degassed under vacuum at 50°C and cured successively at 80°C for 10 h and 150°C for 2 h.

2.2. Measurements

2.2.1. Differential scanning calorimetry (DSC)

The calorimetric measurements were made on a Perkin–Elmer Pyris 1 differential scanning calorimeter in a dry nitrogen atmosphere. Indium and tin standards were used for calibration for low and high temperature regions, respectively. The sample weight used in the DSC pan was about 12 mg; the heating rate was 20°C/min. The midpoint of the slope change of the heat capacity plot of the second heating scan was taken as the glass transition temperature (T_g).

2.2.2. Dynamic mechanical analysis (DMA)

Dynamic mechanical measurements were carried out on a Rheometrics SRA II solids analyzer. The frequency used was 1.0 Hz, and the heating rate was 3.0°C/min. Specimen dimensions were $2.2 \times 0.5 \times 0.05$ cm.

2.2.3. Scanning electron microscopy (SEM)

To investigate the phase structure of the cured ER/SB blends, the specimens were fractured under cryogenic conditions using liquid nitrogen. The fractured surface was immersed in THF at room temperature for 20 h. The SB phase and/or the sol fraction of the epoxy network were preferentially etched by the solvent while the cured ER phase remained relatively unaffected. The etched samples were then dried to remove the solvent. The observation was made on an ElectroScan environmental system 2020 scanning electron microscope. Before observation, the surfaces were coated with a thin gold layer of about 20 nm thickness.

2.2.4. Transmission electron microscopy (TEM)

Samples were microtomed at −100°C with a Leica EMFCS instrument equipped with a diamond knife. The resulting ultrathin sections of 70–100 nm thick were picked up on copper grids and stained in the vapor of an aqueous solution of RuO_4. Stained samples were imaged in a LEO Omega 912 transmission electron microscope (TEM) with an accelerating voltage of 120 kV.

2.2.5. Small-angle X-ray scattering (SAXS)

The small angle X-ray scattering (SAXS) experiments were performed with a Kratky compact camera (Anton Paar K.G., Graz, Austria) at room temperature. The CuKα radiation from a sealed X-ray tube was reflected from a

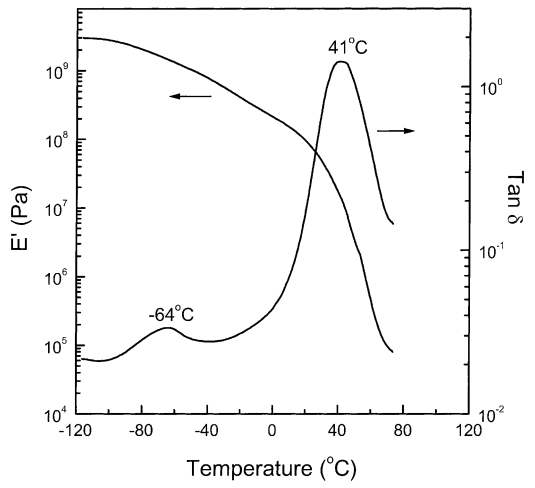

Fig. 1. Dynamic mechanical properties of the cured ER as a function of temperature.

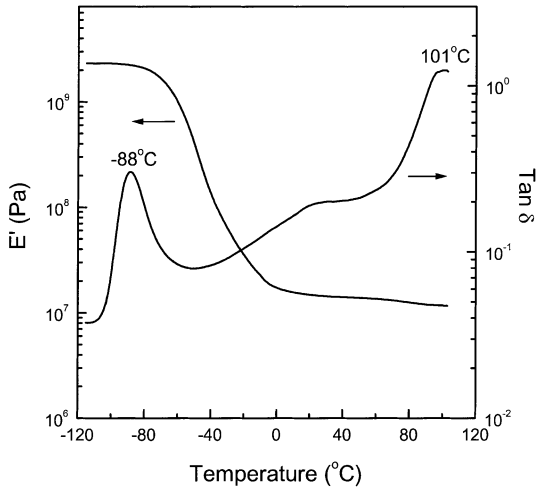

Fig. 2. Dynamic mechanical properties of the SB diblock copolymer as a function of temperature.

graphite monochromator. The range of scattering vector $s = 2 \sin \theta/\lambda$, where $\lambda = 0.154$ nm is the wavelength and 2θ the scattering angle, was 0.01–0.3 nm^{-1}. The scattered intensity was recorded with a scintillation counter in a step-scanning mode. The sample was placed in a brass sample holder with acetate windows. The holder together with the collimation system was seated in an evacuated chamber. The background was corrected by subtraction of the scattering from an empty sample holder. The intensity was normalized to the incoming flux with the help of a moving slit device. The effect of the slit-like cross section of the beam was accounted for by desmearing the data using the standard procedure [32].

3. Results and discussion

3.1. Miscibility of DDM-cured ER/SB blends

3.1.1. Dynamic mechanical properties

Dynamic mechanical properties of DDM-cured ER (Fig. 1) show two typical relaxation peaks of the epoxy network. They are centered at 41 and −64°C and designated by α and β relaxations, respectively. The α relaxation is associated with the glass transition. The β relaxation, of a relative low amplitude, is attributed to motions of poly(propylene oxide) chains in the network.

Dynamic mechanical properties of the SB diblock copolymer are shown in Fig. 2. Two well defined relaxation peaks are observed at 101 and −88°C, corresponding to two glass transitions, characteristics of the respective homopolymers, polystyrene (PS) and polybutadiene (PB). These relaxations are in good agreement with those reported in the literature [33,34].

Dynamic mechanical properties of the cured ER/SB blends of different compositions were also studied. The modulus vs T curves of the blends are relative featureless. Tan δ vs T curves of the ER, SB and several cured ER/SB blends are shown in Fig. 3. For the blends, three separate relaxation peaks are observed around 101, 41 and −88°C, respectively corresponding to the glass transitions of a PS microphase (T_{gPS}), an ER-rich phase (T_{gER}) and a PB microphase (T_{gPB}). The positions of all the three glass transitions remain almost unchanged with the blend composition. Fig. 4 summarizes the values of T_{gPS}, T_{gER} and T_{gPB} as a function of the blend composition for all the blends studied. The existence of three separate glass transitions, whose values are independent of the blend composition, indicates that SB is immiscible with the cured ER. Neither the PS block nor the PB block exhibits miscibility with the cured ER. The SB diblock copolymer is microphase separated in the macroscopically phase separated ER/SB blends; there exhibit three phases in the blends, i.e. a PS microphase, an ER-rich phase and a PB microphase.

3.1.2. DSC

The samples of all the cured blends were subjected to DSC measurement. Fig. 5 shows DSC thermogams of the ER, SB and the cured ER/SB blends. All the cured blends show a glass transition located around 30°C, which corresponds to that of cured ER phase in the blends. For the blends with 50 wt% SB or more, another glass transition appears around 90°C, corresponding to that of the PS microphase in the blends. However, glass transition of the PB microphase in the blends and in the plain SB cannot be detected at the used experimental conditions. The T_g values obtained with DSC are also summarized in Fig. 4 as a function of blend composition. In the figure, the T_g values obtained from DMA are generally about 10°C higher than those from DSC at the same compositions as expected.

It has been known that the relationship between the T_g and composition in ER/linear polymer blends is indicative of the extent of phase separation and the crosslinking of ER [3,5,6]. The considerable lowering of the T_g of the ER

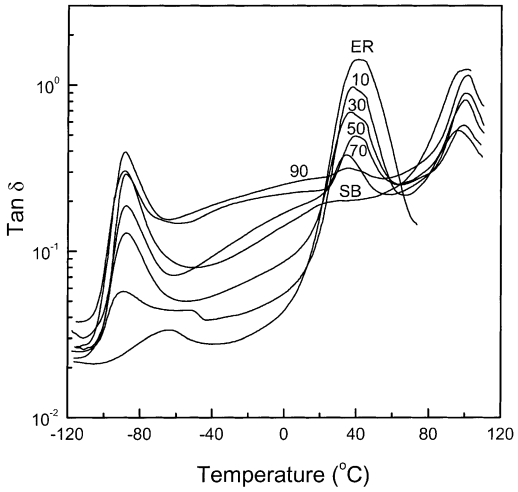

Fig. 3. Temperature dependence of tan δ of ER/SB blends. The figures indicate the respective SB content in weight percent in the blends.

phase is generally observed for cured ER/thermoplastic blends. The incomplete phase separation between the thermoplastic and the crosslinked ER may cause a depression in T_g of the cured ER phase. This phenomenon is due to the fact that crosslinking density is much reduced in the blend as ER concentration is decreased. The curing reaction of ER involves chain extension, branching and crosslinking. In an ER/thermoplastic blend, as the curing reaction proceeds, the molecular weight of the system greatly increases and the crosslinking network structure in three-dimension forms. Curing reaction can induce phase separation in an initially miscible ER/thermoplastic blend [6], and there exists a competitive progress between the phase separation and the crosslinking reaction during the cure process. The dilution effect of the thermoplastic gives rise to an incomplete curing

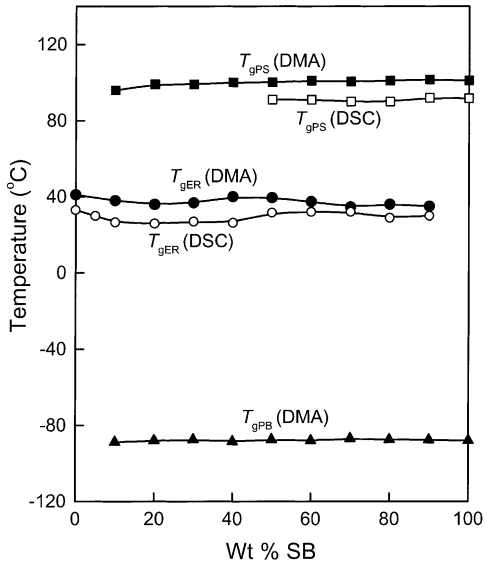

Fig. 4. Glass transition behavior of ER/SB blends. The filled symbols denote the T_g values obtained by DMA; the open symbols represent those obtained by DSC.

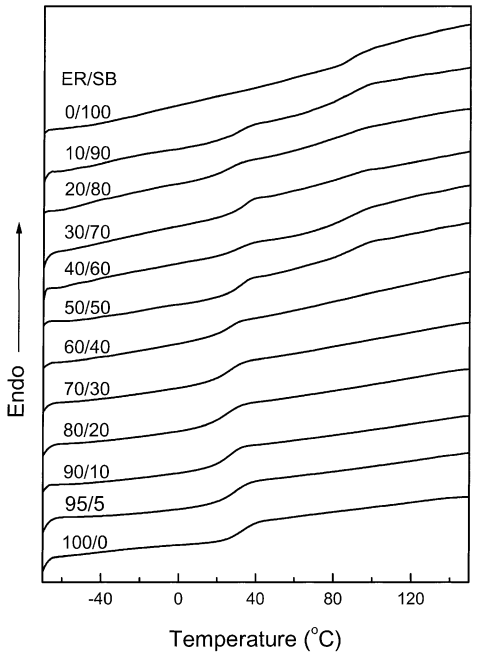

Fig. 5. DSC thermograms of the second scan of ER/SB blends.

reaction in the blend, and thus a lower T_g for the ER crosslinked network. Furthermore, the addition of the thermoplastic raises the viscosity of the system, which may result in an incomplete curing reaction due to the kinetic factor [23]. On the other hand, the occurrence of crosslinking causes dramatic changes in the chemical and physical nature of the system. Ayll of these factors give rise to the occurrence of phase separation between the thermoplastic component and the crosslinked ER matrix in ER/thermoplastic blends.

It can be seen from Fig. 4 that three T_g values of the blends, both by DMA and DSC, are all approximately equal to those of the pure components, respectively. This indicates that the phase separation in thermoset/TPE blends of ER with SB is quite complete, and hence the crosslinking of the ER is quite complete in the blends. All the DDM-cured ER/SB blends were opaque or translucent, indicating the occurrence of phase separation. It was noted that the uncured ternary mixtures of PPGDGE, SB and DDM cast from THF were not completely transparent, suggesting that phase separation could have taken place to some extent before the curing reaction occurred. This is different from the reaction-induced phase separation in ER/thermoplastic blends.

3.2. Phase morphology of DDM-cured ER/SB blends

3.2.1. ER/SB blends with SB content up to 30 wt%

The morphology of the cured blends was investigated by SEM. The SEM micrographs of cryogenically fractured surfaces of 95/5, 90/10, 80/20 and 70/30 ER/SB blends are presented in Fig. 6. The heterogeneous morphology is

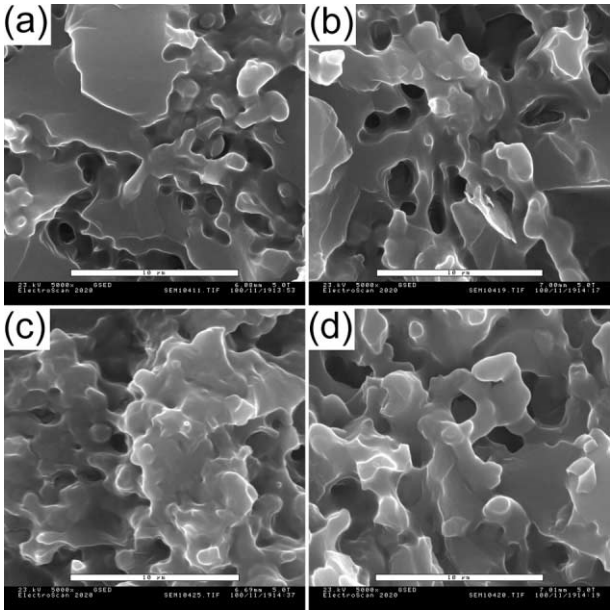

Fig. 6. SEM micrographs of cryogenically fractured surfaces of (a) 95/5, (b) 90/10, (c) 80/20, and (d) 70/30 ER/SB blends. Scale bars are 10 μm.

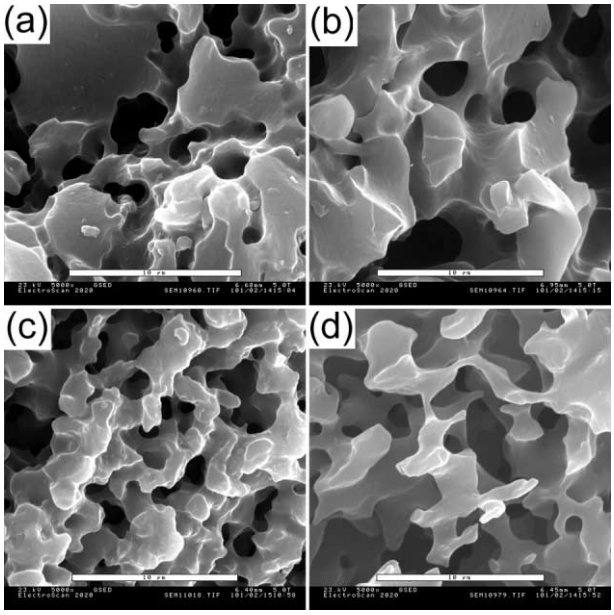

Fig. 7. SEM micrographs of fractured surfaces of (a) 95/5, (b) 90/10, (c) 80/20, and (d) 70/30 ER/SB blends etched with THF for 20 h. Scale bars are 10 μm.

observed in all the cases, which supports the results of DSC and DMA that these blends are phase separated. To enable further examination to take place, the fractured surfaces of the specimens were etched with THF to remove SB, so that the morphology of the specimens may be more clearly shown. The SEM micrographs of the etched specimens of these blends are given in Fig. 7, displaying characteristics of a phase-separated structure. For the 95/5 ER/SB blend, the SB domains with irregular shapes and broadly distributed sizes are dispersed in a continuous cured ER matrix (Fig. 6(a)). A structure of the order of 2–5 μm is obtained. The SEM micrograph for the etched specimen of 95/5 ER/SB blend clearly shows vacant holes with irregular shapes in the ER matrix after the SB phase was rinsed away by THF (Fig. 7(a)).

With increasing SB content, the morphology of the cured blends changes gradually. The 90/10 ER/SB blend gives rise to a similar morphology for the fractured surfaces. The SEM micrograph of the etched specimen further displays vacant holes with irregular shapes but larger sizes in the ER matrix (Fig. 7(b)); a phase structure with size of the order of about 5 μm is obtained. The morphology observed for the 95/5 and 90/10 ER/SB blends could be a combined one intermediate between the SB dispersed and the bicontinuous phase structures. A similar morphology was reported in trifunctional ER/polyetherimide (PEI) blends when the PEI concentration was 15 wt% by Hourston and Lane [26].

Fig. 8(a) displays TEM micrograph of 90/10 ER/SB blend at low magnification. The dark domains are SB dispersed phase because the PS block in SB diblock copolymer was preferentially stained with RuO_4. TEM micrograph of 90/10 ER/SB blend at a higher magnification is further presented in Fig. 8(c). It can be seen from Fig. 8 that the two phases are well bounded and there is a good interfacial adhesion between the SB domains and the ER continuous phase.

When the SB content rises to 20 wt%, SB domains are highly coagulated in a continuous ER phase (Fig. 6(c)). The SEM micrograph of the etched specimen (Fig. 7(c)) further reveals that the 80/20 ER/SB exhibits an interpenetrating network phase structure, i.e. an interpenetrating bicontinuous phase structure with an SB skeletal element in the ER continuous phase. Fig. 7(c) clearly displays characteristics of three-dimensional continuity of both phases. The void areas clearly show the form of the skeletal SB phase, which was extracted away with THF, and the antitropic ER matrix. The size of phase structure is observed to be of the order of 2–5 μm. These characteristics were examined by TEM observation. TEM micrograph shown in Fig. 8(b) can be taken as a two-dimensional projection of a three-dimensional interpenetrating bicontinuous phase structure. However, the two continuous phases exhibit some topological characteristic differences. The SB phase (dark areas) seems to be primarily convex, forming a network of the SB phase, i.e. a 'skeletal' structure, while the cured ER phase then occupies the space around the SB phase and presents a 'matrix' characteristic. The ER matrix, i.e. the surrounding phase, takes the opposite, concave surface at the interface. Fig. 8(b) clearly shows that SB skeletal phase was formed in the continuous ER phase. Fig. 8(d) presents TEM micrograph of 80/20 ER/SB blend at a higher magnification, showing a good interfacial adhesion between the two phases.

For 70/30 ER/SB blend, an ideal interpenetrating bicontinuous phase morphology was formed, i.e. the two separated phases were simultaneously continuous (Fig. 6(d)). It can clearly be seen from the SEM micrograph of the etched

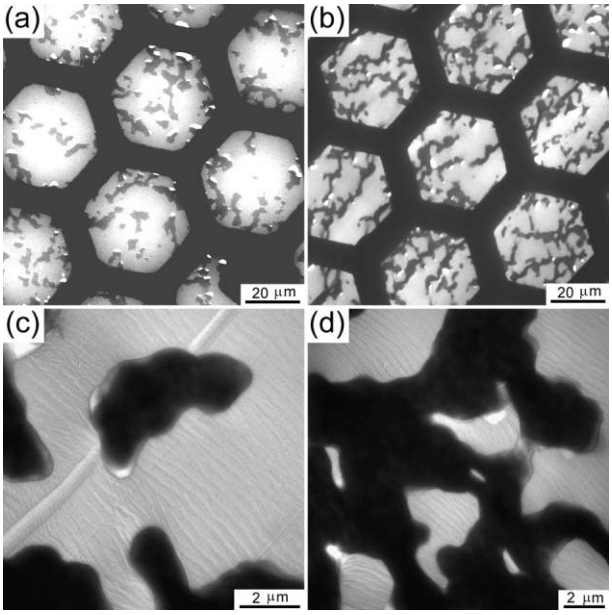

Fig. 8. TEM micrographs of 90/10 and 80/20 ER/SB blends. The top two micrographs ((a) and (b)) are taken at low magnification. The left two micrographs ((a) and (c)) are for 90/10 ER/SB blend, the right two ((b) and (d)) for 80/20 ER/SB blend. Note that the striations with spacing ≈ 0.4 μm appearing in parts (c) and (d), as well as the trace perpendicular to the striations in part (c) are artifacts introduced by the ultrathin sectioning processes.

specimen in Fig. 7(d) that a perfect three-dimensional spatially bicontinuous structure was developed. Both concave and convex surfaces and interlocking and continuous phases can be seen; the two complementary continuous phases are topologically identical. The size of phase structure is of the order of about 5 μm.

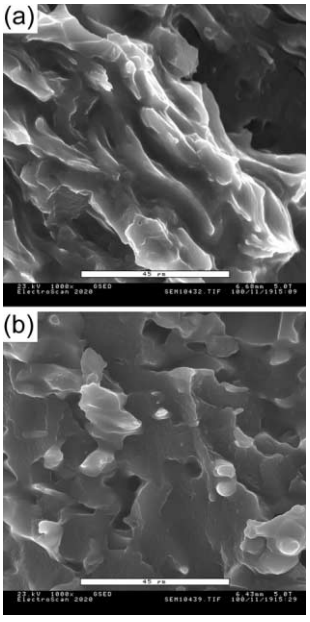

Fig. 9. SEM micrographs of cryogenically fractured surfaces of (a) 60/40 and (b) 40/60 ER/SB blends. Scale bars are 45 μm.

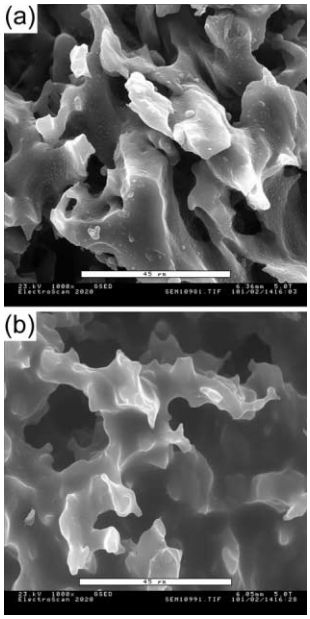

Fig. 10. SEM micrographs of fractured surfaces of (a) 60/40 and (b) 40/60 ER/SB blends etched with THF for 20 h. Scale bars are 45 μm.

Bicontinuous phase structures where each of the two polymers has three-dimensional spatial continuity can be obtained in binary blends through the application of correct methods of mixing [35–37]. Interfacial tension between the incompatible polymer components drives the system toward minimum surface free energy, i.e. toward phase growth. Formation of the network structure within both continuous phases kinetically inhibits further phase growth or phase retraction. This inhibition may be achieved by chemical or physical crosslinking. Crosslinking would provide a kinetic barrier to further phase separation to the late stage of demixing, e.g. coarsening process that may result in breakup of the bicontinuous phase structure. In the present ER/SB blends, chemical crosslinking of the ER matrix prevents the breakup of the SB continuous phase into droplets that would form a dispersed phase. The SB phase with a much higher viscosity at the initial stage of the curing reaction became the skeletal component with convex surface. Curing of the ER phase results in a continuous crosslinked ER matrix.

3.2.2. ER/SB blends with 40–60 wt% SB

The SEM micrographs of cryogenically fractured surfaces of 60/40 and 40/60 ER/SB blends are presented in Fig. 9. The two-phase morphology can be observed in both the cases; and phase separation took place during the preparation of the blends. Fig. 10 presents SEM micrographs of etched surfaces of the fractured specimens. The SB phase was removed with THF but the cured ER phase remained, the morphology of the specimens is more clearly shown. The phase morphology shown in these photographs is typical of interpenetrating bicontinuous phase structure. The complementary bicontinuous networks are obtained.

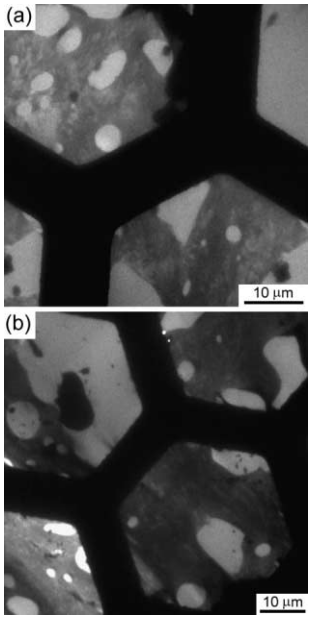

Fig. 11. TEM micrographs of (a) 60/40 and (b) 40/60 ER/SB blends.

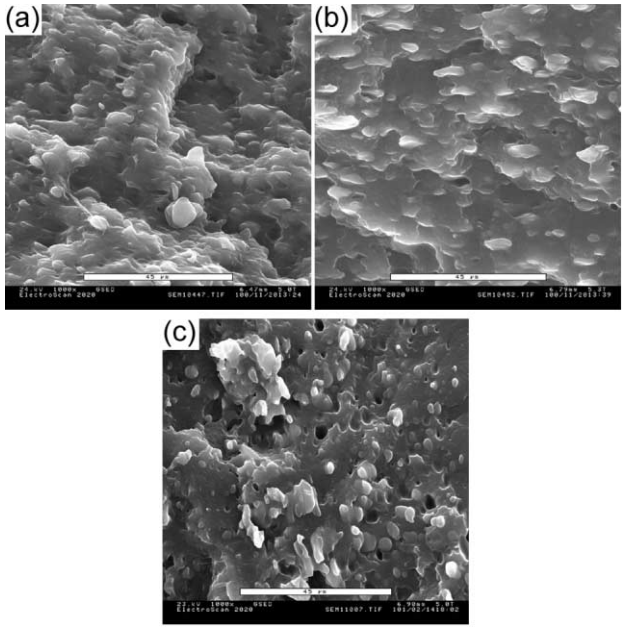

Fig. 12. SEM micrographs of cryogenically fractured surfaces of (a) 30/70, (b) 20/80, and (c) 10/90 ER/SB blends. Scale bars are 45 μm.

However, the size of phase structure is of the order of 20–30 μm, that is substantially increased. It can be seen from Fig. 10(b) that the morphology of 40/60 ER/SB blend is more chaotic than any perceived minimal surface that may be present. TEM micrographs of 60/40 and 40/60 ER/SB blends at low magnification are given in Fig. 11, displaying obvious characteristics of a phase-separated structure for both the blends. The dark areas are SB phase whereas the white ones are cured ER phase. The TEM observation confirms that both the blends have a bicontinuous phase structure. It can also be seen that some smaller white areas with sizes of the order of 2–10 μm, which are discrete ER domains, are dispersed within the continuous SB phase. Meanwhile, only a few discrete SB domains are dispersed in the continuous ER matrix.

It is interesting to notice that the ER/SB blends exhibit a bicontinuous phase structure in a broad range of composition, i.e. with SB content from 20 to 60 wt%. This corresponds to an SB volume content from 23 to 64 vol% with $\rho_{SB} = 0.940$ g/cm^3 and $\rho_{ER} = 1.115$ g/cm^3. The value of ρ_{ER} is calculated by the group contribution approach [38]. It is noted that the size of phase structure shows a remarkable increase, from an order of 2–5 μm to that of 20–30 μm, as the SB content is increased from 20 to 60 wt%. This can be interpreted as a result of the competitive progress between the phase separation and the curing reaction during the preparation process of the blends. The rate of curing reaction in the ER/SB blends decreases with increasing SB content because of the dilution effect of SB. The higher the SB content in the blend, the longer the period of time to achieve a crosslinked network phase structure that can effectively inhibit further phase separation or retraction during the curing process, and hence the larger the size of phase structure developed.

3.2.3. ER/SB blends with 70 wt% and more SB

When the SB content is increased to 70 wt%, i.e. 73.5 vol%, phase inversion occurs. Fig. 12 shows SEM micrographs of cryogenically fractured surfaces of 30/70, 20/80 and 10/90 ER/SB blends. They clearly show phase-separated structure for these blends. The ER particles are wrapped in the SB continuous phase. TEM micrographs of these blends in Fig. 13 obviously display a phase-inverted morphology. The ER domains (white areas) are dispersed in the SB thermoplastic elastomer continuous phase (dark region). It can be seen from Figs. 12 and 13 that the ER domain size slightly decreases with decreasing ER content. The average size for the ER dispersed domains are of the order of about 5 μm for the 30/70 and 20/80 ER/SB blends. For the 10/90 blend, only some discrete ER particles with size of 2–5 μm are dispersed within the continuous SB phase.

The SEM and TEM observations presented above have clearly shown that all the ER/SB blends possess a two-phase morphology, indicating the immiscibility of the components as revealed by DMA and DSC studies. The phase morphology is dependent on the blend composition. Phase separation process in ER/thermoplastic blends has been studied extensively [5,6]; the spinodal decomposition (SD), the nucleation growth (NG), or the mixed mode of both can occur. During the process of phase transformation, the morphology of a blend is determined by the competition between the rate of curing and rate of phase separation. Phase separation is inhibited when the blend is at high viscosity, gelation, or vitrification, and result in none or incomplete phase separation; the diffusion rate thus becomes the dominant factor on the final cured morphology.

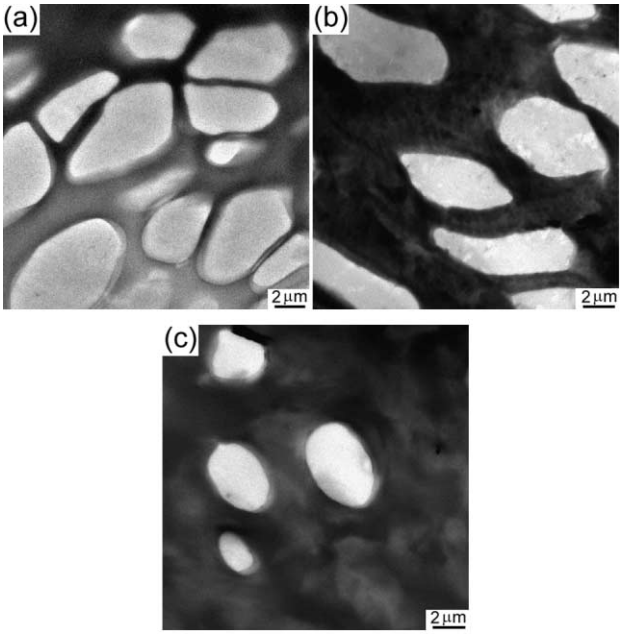

Fig. 13. TEM micrographs of (a) 30/70, (b) 20/80, and (c) 10/90 ER/SB blends.

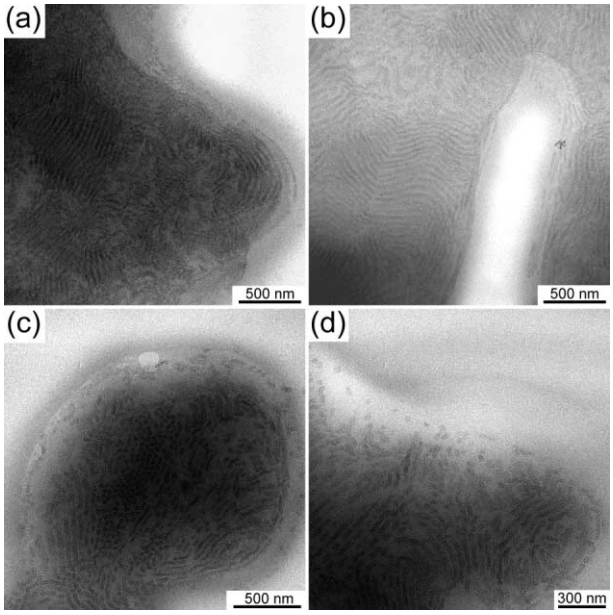

Fig. 14. TEM micrographs of 80/20 ER/SB blend. Note the scale bar in part (d) is different.

For the blends with 5 and 10 wt% SB, the morphology could be formed through a mixed mode of both the SD mechanism and the NG mechanism. The appearance of interpenetrating bicontinuous phase structures for the blends with SB content from 20 to 60 wt% implies that phase separation followed the SD mechanism during preparation of the blends. For the blends with 70 wt% and more SB, dispersion of cured ER particles in the SB matrix suggests that phase separation occurred by the NG mechanism.

3.3. Interfacial and microphase structures of DDM-cured ER/SB blends

In phase-separated polymer blends, the interfacial structure plays an important role because it controls the adhesion between the different phases as well as the phase morphology of the blends [39–41]. The final mechanical properties of the blends are strongly dependent on their interfacial structure. To investigate the interfacial and microphase structures of DDM-cured ER/SB blends, the morphology of the blend samples was studied by TEM at high magnifications.

Fig. 14 displays TEM micrographs of 80/20 ER/SB blend showing the interfacial region and internal structure of the SB phase. All the TEM micrographs clearly show lamellar microphase structure within the SB phase. Note that RuO_4 preferentially stains PS blocks in the SB diblock copolymer. The PS microphase appears dark in the TEM micrographs. However, it is not possible to discern the PB microphase and the ER phase by staining with RuO_4. It has been shown in Section 3.2 that the 80/20 ER/SB blend exhibits an interpenetrating bicontinuous phase structure with an SB skeletal element in the ER continuous phase. This characteristic of the phase structure results in several types of phase and interfacial morphology as can be seen from the TEM micrographs in Fig. 14. Fig. 14(a) presents a TEM micrograph showing white ER phase, dark SB phase and the internal microphase structure of SB phase, as well as the interfacial layer between the ER and SB phases. Inside the SB phase, lamellae of about 45 nm thick are observed. An interfacial layer between the SB and ER phases, which varies from 200 to 300 nm in thickness, is identified. The appearance of the interfacial layer is not uniform. It can be seen that the interfacial layer appears dark adjacent to the SB phase but gradually becomes lighter from the SB phase to the ER phase. TEM observation also reveals that there exists some discrete ER domains within the continuous SB phase (Fig. 14(b)). Lamellae of 45–50 nm thick are observed within the dark SB continuous phase in Fig. 14(b). The interfacial layer between the SB and ER phases varies from 100 to 200 nm in thickness, substantially thinner than that presented in Fig. 14(a).

Fig. 14(c) shows the detailed structure of a nearly isolated SB domain and its interfacial region observed for 80/20 ER/SB blend. The figure clearly shows both lamellae and cylinders inside the SB domain. It is interesting to see that the interfacial region between the SB and ER phases consists of both an outer layer and an inner layer. The thickness of the outer layer is about 100 nm whereas that of the inner layer varies from 100 to 200 nm. Note that SB micelles can be found in the inner layer and the size of the micelles is about 20 nm in diameter.

Fig. 14(d) shows a TEM micrograph observed for 80/20 ER/SB blend at an even higher magnification. The detailed structure of SB phase and the interfacial layer are clearly

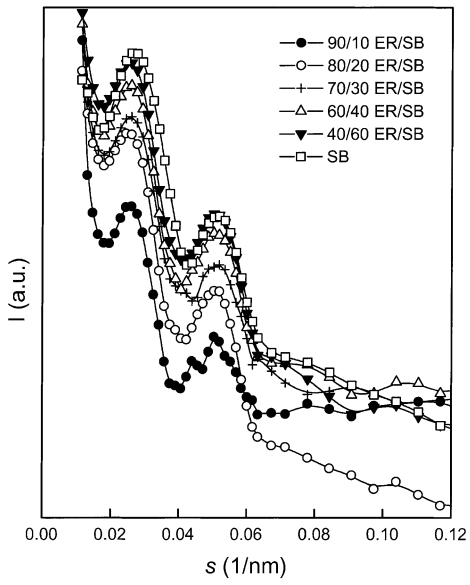

Fig. 15. Desmeared SAXS patterns of DDM-cured ER/SB blends. The scattering vector $s = 2 \sin \theta/\lambda$. $\lambda = 0.154$ nm is the wavelength and 2θ the scattering angle.

displayed. The SB phase shows a lamellar morphology. However, some lamellae are broken up into droplets in the SB phase. The interface between the phases is more diffusive; SB micelles are formed surrounding the SB phase.

The TEM observation presented here clearly reveals that a good interfacial adhesion exists between the SB and ER phases in the blends. The SB comprises PS and PB blocks. The solubility parameters of PB, PS and the ER are calculated by using Hoy's group contribution constants to be 17.5, 19.1 and 20.9 $(J/cm^3)^{1/2}$, respectively [38,42]. It is noticed that PS has a solubility parameter closer to that of the ER than PB does. Obviously, the repulsive interaction between PB block and the ER makes the interface between PB and the ER possess a high interfacial free energy. In contrast, the formation of interface between PS and the ER would apparently decrease the free energy. Therefore, the PS block of SB in the interface region is expected to accompany with the surrounding ER matrix. It is reasonable to assume that the PB blocks aggregate the core of the SB micelle and the PS blocks form the shell of the micelle; the latter is surrounded by the ER matrix in the blend [43].

SAXS measurements have been performed for samples of plain SB and ER/SB blends to characterize their microphase structures. Desmeared SAXS patterns for the SB and several ER/SB blends are shown in Fig. 15. For the plain SB block copolymer, the main peak is centered at a value of the scattering vector s corresponding to a long spacing of 37.3 nm. There is a second-order reflection clearly visible at double angular position of this first-order maximum. Such a sequence is characteristic of an arrangement of lamellae. Similar SAXS scattering patterns are observed for the ER/SB blends with SB content from 10 to 60 wt%. The main peaks for these blends appear at s values corresponding to distances in real space between 38.5 and 39.7 nm which are long spacings of the lamellar structure within the SB phase. It is noted that the long spacings of the lamellae obtained here by SAXS are smaller than those obtained from the TEM micrographs in Fig. 14 for 80/20 ER/SB blend. This result implies that the ultrathin sections are not normal to the plane of the lamellae in the blend. The SAXS results presented here further reveal that the SB diblock copolymer still exhibits a lamellar microphase structure within the SB phase in the macroscopically phase separated ER/SB blends. The long spacing of the lamellae nearly does not change in the blends.

4. Conclusions

The SB diblock copolymer is immiscible with DDM-cured PPG-type ER, and there exist three separate glass transitions in the cured ER/SB blends. The values of the T_gs are independent of the blend composition; neither the PS block nor the PB block exhibits miscibility with the cured ER. The blends exhibit three phases, i.e. a PS microphase, an ER-rich phase and a PB microphase. A variety of morphologies can be achieved, depending on the blend composition. For the blends with 5 and 10 wt% SB, SB domains with irregular shapes and broadly distributed sizes are dispersed in the continuous cured ER matrix. For the blends with 20–60 wt% SB, an interpenetrating bicontinuous phase structure is formed. For the blends with 70 wt% and more SB, ER particles are dispersed in the SB matrix. A good interfacial adhesion is present between the SB and ER phases in the blends. The interfacial layer between the ER and SB phases varies from 100 to 300 nm, and SB micelles are formed surrounding the SB phases for the blend with 20 wt% SB content. The SB diblock copolymer is microphase separated in the macroscopically phase separated ER/SB blends. The lamellar microphase structure presents within the SB phase and the long spacing of lamellae remains almost unchanged in the blends.

Acknowledgements

The authors are indebted to Dr Y. Thomann for help in using the microtome instrument, Mrs B. Heck for assistance in the SAXS measurements and Mr R. Landers for the SEM observation. Q.G. would like to express his gratitude to the Alexander von Humboldt-Stiftung for awarding the prestigious Humboldt Research Fellowship.

References

[1] Riew CK, Gillham JK, editors. Rubber-modified thermoset resins. Advances in chemistry series number 208. Washington DC: ACS, 1984.

[2] Riew CW, editor. Rubber-toughened plastics. Advances in chemistry series number 222. Washington DC: ACS, 1989.
[3] Riew CK, Kinloch AJ, editors. Toughened plastics I: science and engineering. Advances in chemistry series number 233. Washington DC: ACS, 1993.
[4] Riew CK, Kinloch AJ, editors. Toughened plastics II: novel approaches in science and engineering. Advances in chemistry series number 252. Washington DC: ACS, 1996.
[5] Guo Q. In: Shonaike GO, Simon G, editors. Polymer blends and alloys, vol. 6. New York: Marcel Dekker, 1999. p. 155–87.
[6] Inoue T. Prog Polym Sci 1995;20:119.
[7] Noshay A, Robeson LM. J Polym Sci Polym Chem Ed 1974;12:689.
[8] Clark JN, Daly JH, Garton A. J Appl Polym Sci 1984;9:3381.
[9] Guo Q, Peng X, Wang Z. Polymer 1991;32:53.
[10] Mucha M. Colloid Polym Sci 1994;272:1090.
[11] Zheng H, Zheng S, Guo Q. J Polym Sci Polym Chem Ed 1997;35:3161.
[12] Zhong Z, Guo Q. Polymer 1998;39:517.
[13] Hillmyer MA, Lipic PM, Hajduk DA, Almdal K, Bates FS. J Am Chem Soc 1998;120:8963.
[14] Lipic PM, Bates FS, Hillmyer MA. J Am Chem Soc 1998;120:8963.
[15] Horng TJ, Woo EM. Polymer 1998;39:4115.
[16] Cheng JL, Chang FC. Macromolecules 1999;32:5348.
[17] Mijovic J, Shen M, Sy JW. Macromolecules 2000;33:5235.
[18] Guo Q, Harrats C, Groeninckx G, Koch MHJ. Polymer 2001;42:4127.
[19] Manzione LT, Gillham JK, McPherson CA. J Appl Polym Sci 1981;26:889.
[20] Enns JB, Gillham JK. J Appl Polym Sci 1983;28:2567.
[21] Bucknall CB, Partridge IK. Polymer 1983;24:639.
[22] Bucknall CB, Davies P, Partridge IK. Polymer 1985;26:109.
[23] Bucknall CB, Partridge IK. Polym Eng Sci 1986;26:54.
[24] Verchere D, Sautereau H, Pascault JP, Moschiar SM, Riccardi CC, Williams RJJ. Polymer 1989;30:107.
[25] Verchere D, Pascault JP, Sautereau H, Moschiar SM, Riccardi CC, Williams RJJ. J Appl Polym Sci 1991;42:701.
[26] Hourston DJ, Lane JM. Polymer 1992;33:1397.
[27] Zheng S, Hu Y, Guo Q, Wei J. Colloid Polym Sci 1996;274:410.
[28] Zheng S, Wang J, Guo Q, Wei J, Li J. Polymer 1996;37:4667.
[29] Huang P, Zheng S, Huang J, Guo Q, Zhu W. Polymer 1997;38:5565.
[30] Song X, Zheng S, Huang J, Zhu P, Guo Q. J Mater Sci 2000;35:5613.
[31] Pascault JP, Williams RJJ. In: Paul DR, Bucknall CB, editors. Polymer blends, Vol. 1. Formulation. New York: Wiley, 2000. p. 379–415, Chapter 13.
[32] Strobl G. Acta Crystallogr 1970;A26:367.
[33] Sardelis K, Michels HJ, Allen G. Polymer 1987;28:244.
[34] Valenti B, Turturro A, Losio S, Falqui L, Costa G, Cavazza B, Castellano M. Polymer 2001;42:2427.
[35] Gergen WP, Lutz RG, Davison S. In: Legge NR, Holden G, Schroeder HE, editors. Thermoplastic elastomers. Munich: Hans Publishers, 1987. p. 507–40, Chapter 14.
[36] Jinnai H, Koga T, Nishikawa Y, Hashimoto T, Hyde ST. Phys Rev Lett 1997;78:2248.
[37] Jinnai H, Hashimoto T, Lee D, Chen SH. Macromolecules 1997;30:130.
[38] Van Krevelen DW. Properties of polymers. 3. Amsterdam: Elsevier Science, 1990.
[39] Fayt R, Jerome R, Teyssie Ph. J Polym Sci Polym Lett Ed 1986;24:25.
[40] Datta S, Lohse DJ. Macromolecules 1993;26:218.
[41] Lyu SP, Cernohous JJ, Bates FS, Macosko CW. Macromolecules 1999;32:106.
[42] Hoy KL. J Paint Technol 1970;42:76.
[43] Polance R, Nichols K, Jayaraman K. Polymer 1994;35:5051.